



# Visible-light-driven graphene supported Cu/Pd alloy nanoparticle-catalyzed borylation of alkyl bromides and chlorides in air



Zhi-Feng Jiao<sup>a</sup>, Ya-Ming Tian<sup>b</sup>, Xiao-Ning Guo<sup>b,\*</sup>, Udo Radius<sup>b</sup>, Holger Braunschweig<sup>b</sup>, Todd B. Marder<sup>b</sup>, Xiang-Yun Guo<sup>a</sup>

<sup>a</sup>Jiangsu Key Laboratory of Advanced Catalytic Materials and Technology, School of Petrochemical Engineering, Changzhou University, Changzhou 213164, China

<sup>b</sup>Institute of Inorganic Chemistry, and Institute for Sustainable Chemistry & Catalysis with Boron, Julius-Maximilians-Universität Würzburg, Am Hubland, 97074 Würzburg, Germany

## ARTICLE INFO

### Article history:

Received 22 October 2020  
Revised 21 December 2020  
Accepted 16 January 2021  
Available online 23 January 2021

### Keywords:

Alkylboronates  
Borylation  
Photocatalysis  
Cu/Pd alloy nanoparticles, localized surface plasmon resonance

## ABSTRACT

A highly efficient photocatalytic protocol for borylation of alkyl bromides and chlorides with graphene supported Cu/Pd alloy nanoparticles as a heterogeneous catalyst is reported. This photocatalytic system operates with visible light in air, providing a wide range of primary and secondary alkyl halides with B<sub>2</sub>pin<sub>2</sub> or B<sub>2</sub>neop<sub>2</sub> in high yields at low temperatures, thereby demonstrating its broad utility and functional group tolerance. The high performance is attributed to a synergistic effect of localized surface plasmon resonance (LSPR) of Cu and charge transfer from Cu to Pd due to the alloy surface charge heterogeneity. Transfer of energetic electrons from Pd to electrophilic alkyl halides lead to the formation of the alkyl radicals, which quickly react with a nucleophilic adduct of a diboron compound with base adsorbed on the positively charged Cu sites to form the corresponding borylation product.

© 2021 Elsevier Inc. All rights reserved.

## 1. Introduction

Organoboron esters are key building blocks in organic synthesis, materials science, and drug discovery [1–10]. Transition metal-catalyzed borylation of alkyl halides, based on Cu [11–19], Zn [20], Ni [21–23], Pd [24], Fe [25,26], and Mn [27], etc., have emerged as a powerful tool for the synthesis of alkylboronate esters. Biscoe et al. developed an efficient C–X borylation protocol that employs Pd<sub>2</sub>(dba)<sub>3</sub> (dba = dibenzylideneacetone) as catalyst for the borylation of primary alkyl bromides, iodides and tosylates [24]. Our group reported the CuI/PPh<sub>3</sub> [12] and ZnCl<sub>2</sub>/NHC [20] (NHC = N-heterocyclic carbene)-catalyzed borylation of alkyl halides with bis(pinacolato)diboron (B<sub>2</sub>pin<sub>2</sub>), giving alkylboronate esters in good to excellent yields. Cook et al. showed that alkyl electrophiles can be borylated using Fe(III) acetoacetate [25] and Mn(II) bromide [27] with tetramethylethylenediamine, applying EtMgBr as a stoichiometric activator. Recently, photoinduced borylations have become attractive due to the enhancement of catalytic efficiency [28–39]. Li et al. employed [Ir(ppy)<sub>2</sub>(dtbpy)]PF<sub>6</sub> as a single electron transfer catalyst to achieve the synthesis of primary and secondary alkyl boronates by visible light-promoted decarboxylative borylation of aliphatic esters [34]. The groups of Aggarwal [40,41], Studer [42–44], Shi [45], Glorius [46], Melchiorre [47], Mo [48], and Jiao

[49] developed a series of photoinduced transition metal-free radical-type borylation reactions by employing reactive alkyl-derived N-hydroxyphthalimide esters, Katritzky salts, xanthates/oxalates and alkyl halides as aliphatic sources to yield alkylboronate esters.

While homogeneous catalytic borylation of alkyl halides has progressed rapidly, heterogeneous catalytic borylation of alkyl halides has progressed slowly, and only a few examples have been published thus far [50–54], mostly involving alkyl iodides and bromides. Sarkar et al. described the nanosized palladium-catalyzed borylation of benzyl halides under solvent- and ligand-free conditions, affording benzyl boronates in high yield [50]. The borylation of the C(alkyl)–Cl bond is still a challenge in the heterogeneous field. In 2016, our group reported an efficient CuCl<sub>2</sub>/NHC-catalyzed-borylation protocol for most primary, secondary, and tertiary alkyl halides, including alkyl chlorides, at room temperature to 60 °C for only 0.5–1 h, even open to air [16]. Very recently, Bose et al. reported a magnetically separable Cu nanocatalyst for the borylation of alkyl and benzyl halides [53]. The procedure is applicable to the borylation of alkyl bromides at room temperature and benzyl halides at 80 °C for 18 h. With primary alkyl chlorides, the reactions were carried out for 24 h at 80 °C. For secondary alkyl chlorides, only chlorocyclohexane was reported with a GC yield of 6%.

Cu nanoparticles exhibit strong visible light absorption due to the localized surface plasmon resonance (LSPR) effect. The LSPR

\* Corresponding author.

E-mail address: [guo.xiaoning@uni-wuerzburg.de](mailto:guo.xiaoning@uni-wuerzburg.de) (X.-N. Guo).

is characterized by a high extinction coefficient for light absorption and large electric fields at the particle surface [55–66], resulting in the formation of energetic charge carriers in the nanoparticles with high efficiency, leading to chemical transformations. Ye et al. developed an efficient plasmonic Cu/ZnO photocatalytic reduction of CO<sub>2</sub> to methanol at ambient pressure [65]. Our previous studies showed that Cu nanoparticles supported on graphene exhibit high photocatalytic activities for the coupling of nitroaromatics [58], aerobic oxidation of amines [60] and *N*-arylation of imidazoles [61] under visible light irradiation. Because photocatalysis has the possibility to generate highly reactive intermediates, and then to achieve reactions that are difficult through conventional ground-state pathways, and studies in both homogeneous and heterogeneous catalysis have shown that Cu works well for the borylation of alkyl halides, we therefore hoped to achieve the borylation of alkyl halides using Cu nanoparticles as the photocatalyst.

## 2. Experimental

### 2.1. General information

All reagents were purchased from Energy Chemical, Aladdin, Alfa-Aesar, Aldrich or ABCR, and were checked for purity by GC-MS and/or <sup>1</sup>H NMR spectroscopy and used as received.

### 2.2. Preparation of Cu<sub>2.8</sub>Pd<sub>0.2</sub>/graphene

The Cu<sub>2.8</sub>Pd<sub>0.2</sub>/graphene catalyst was prepared by a high-temperature liquid-phase oleylamine reduction method. Briefly, 8.8 mg of [Cu(OAc)<sub>2</sub>·H<sub>2</sub>O] and 97 mg of graphene were added into 50 mL of Pd(NO<sub>3</sub>)<sub>2</sub> oleylamine solution (0.037 mmol/L). After 1 h of sonication, the mixture was heated to 230 °C for 6 h under reflux. After cooling to room temperature, the solid product was then separated, washed and dried to obtain the Cu<sub>2.8</sub>Pd<sub>0.2</sub>/graphene catalyst with Cu loading of 2.8 wt% and Pd loading of 0.2 wt% based on the amount of metal in the precursor. The exact loading of Cu and Pd were determined to be 2.74 wt% and 0.17 wt%, respectively, by inductively coupled plasma-mass spectrometry (ICP-MS, Perkin-Elmer ELAN 5000). Cu<sub>3</sub>/graphene, Cu<sub>2.9</sub>Pd<sub>0.1</sub>/graphene, Cu<sub>2.5</sub>Pd<sub>0.2</sub>/graphene and Pd<sub>3</sub>/graphene were prepared following the same procedures as those for Cu<sub>2.8</sub>Pd<sub>0.2</sub>/graphene, except that different amounts of the corresponding metal salt precursors were used. The subscripts in different catalysts refer to the mass loading level of the corresponding metal.

The microstructures of the catalysts were investigated by high-resolution transmission electron microscopy (HRTEM) and high-angle annular dark field scanning transmission electron microscopy (HAADF-STEM). EELS were collected on a 200-kV ARM 200F STEM under vacuum. X-ray photoelectron spectroscopy (XPS) was measured on a Kratos XSAM800 spectrometer, using an Al K $\alpha$  ( $h\nu = 1486.6$  eV) X-ray source as the excitation source. The crystalline phases were characterized by X-ray diffraction (XRD, Rigaku D-Max/RB). UV-Vis absorption spectra were measured with Al<sub>2</sub>O<sub>3</sub> as the reference using a UV-3600 spectrophotometer (Shimadzu).

### 2.3. Photocatalytic reactions

Unless specified otherwise, the reactions were conducted under air with a pressure of 1 atm. A mixture of 1 mmol of alkyl halides, 2 mmol of LiOtBu, 1.2 mmol of B<sub>2</sub>pin<sub>2</sub> and 15 mg of Cu<sub>2.8</sub>Pd<sub>0.2</sub>/graphene catalyst was dissolved in DMF (10 mL) in a photocatalytic reactor equipped with a magnetic stirring bar. The reaction temperature was set at 30 °C for alkyl bromides and 50 °C for alkyl chlorides, respectively, and controlled by a circulating water bath (RT4 circulator, ASONE). The mixture was stirred at 700 rpm during

the reaction and exposed to a Xenon lamp (PLS-SXE300C/CUV, Beijing Perfect Light Scientific and Technical Co. Ltd). A low-pass optical filter was employed to block light with  $\lambda < 400$  nm. The light intensity was maintained at 0.6 W/cm<sup>2</sup>. The effect of the wavelength of light on catalytic performance was investigated using various low pass optical filters to block light below specific cutoff wavelengths and using various light-emitting diode (LED) lamps with different wavelengths, respectively. For the former, employing a filter with a cut-off wavelength of 450 nm as an example, blocks light with wavelengths < 450 nm (the reaction mixture was irradiated by light with wavelengths between 450 and 800 nm). During this process, the light intensity without filtering for the reaction remained unchanged.

After reaction, the reaction mixture was diluted with dichloromethane (DCM, 10 mL), and filtered through a millipore filter (pore size: 0.22  $\mu$ m), and *n*-dodecane (34 mg, 0.2 mmol) was added as an internal standard. The product yields were determined by gas chromatography-mass spectrometry (GC-MS, BRUKER SCION SQ 456 GC-MS) using *n*-dodecane as the internal calibration standard. The values given are the average of two experiments. The yields were calculated based on the amount of alkyl halide. The residue was purified by column chromatography on silica gel (silica: 200–300; eluant: hexane/ethyl acetate) to isolate the desired product.

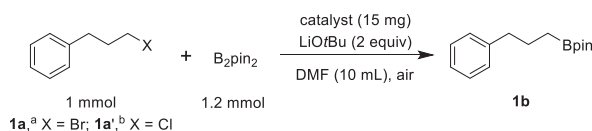
All NMR spectra were recorded at ambient temperature using Bruker DRX-300 (<sup>1</sup>H, 300 MHz; <sup>13</sup>C{<sup>1</sup>H}, 75 MHz) and Bruker Avance III 400 (<sup>1</sup>H, 400 MHz; <sup>13</sup>C{<sup>1</sup>H}, 100 MHz) NMR spectrometers. <sup>1</sup>H NMR chemical shifts are reported relative to TMS and were referenced via residual proton resonances of the corresponding deuterated solvent (CDCl<sub>3</sub>: 7.26 ppm) whereas <sup>13</sup>C{<sup>1</sup>H} NMR spectra are reported relative to TMS via the carbon signals of the deuterated solvent (CDCl<sub>3</sub>: 77.16 ppm). However, signals for the carbon attached to boron, C(aryl)-B, are usually too broad to observe in the <sup>13</sup>C{<sup>1</sup>H} NMR spectra. <sup>11</sup>B NMR chemical shifts are quoted relative to BF<sub>3</sub>·Et<sub>2</sub>O as external standard. <sup>19</sup>F NMR chemical shifts are quoted relative to CFCl<sub>3</sub> as the external standard. All <sup>13</sup>C NMR spectra were broad-band <sup>1</sup>H decoupled. HRMS were measured on a Thermo Scientific Exactive Plus equipped with an Orbitrap. ESI measurements were conducted using a HESI Source with an aux-gas temperature of 50 °C. Measurements were conducted using an APCI Source with a Corona Needle; aux-gas temperature was 400 °C.

### 2.4. EPR measurements

For EPR measurements, 0.2 mmol of 3-phenylpropyl bromide, 0.24 mmol of B<sub>2</sub>pin<sub>2</sub>, 0.4 mmol of LiOtBu, 0.4 mmol of DMPD, 3 mg of Cu<sub>2.8</sub>Pd<sub>0.2</sub>/graphene, and 5 mL of DMF were mixed and placed in a quartz reactor. The mixture was irradiated by a PE300BF Xe lamp source with a light intensity of 0.8 W/cm<sup>2</sup> for 3 min, and then the EPR measurement at X-band (9.86 GHz) was carried out using a Bruker EMXPLUS10/12 EPR spectrometer at room temperature. Another EPR measurement was also conducted using the same method, but without the Cu<sub>2.8</sub>Pd<sub>0.2</sub>/graphene catalyst.

## 3. Results and discussion

Graphene-supported Cu nanoparticles with a 3 wt% loading level (Cu<sub>3</sub>/graphene) were prepared by a liquid reduction method, and were employed for the borylation of 1-bromo-3-phenylpropane (**1a**) and 1-chloro-3-phenylpropane (**1a'**) with B<sub>2</sub>pin<sub>2</sub> at 30 °C in air under irradiation by a Xe lamp with a wavelength range of 400 to 800 nm, which gave 40% and 22% yields of 1-Bpin-3-phenylpropane (**1b**) after 2 h and 9 h (Table 1, entry 2),

**Table 1**  
Photocatalytic borylation of **1a** and **1a'**

Entry	Catalyst	Xe-lamp(400–800 nm)	Yield of <b>1b</b> (%) <sup>c</sup>	
			from <b>1a</b>	from <b>1a'</b>
1	Cu <sub>3</sub> /graphene	×	12	7
2	Cu <sub>3</sub> /graphene	✓	40	22
3	Cu <sub>2.9</sub> Pd <sub>0.1</sub> /graphene	✓	83	64
4	Cu <sub>2.8</sub> Pd <sub>0.2</sub> /graphene	✓	92	78
5	Cu <sub>2.5</sub> Pd <sub>0.5</sub> /graphene	✓	89	67
6	Cu <sub>2</sub> Pd <sub>1</sub> /graphene	✓	70	51
7	Pd <sub>3</sub> /graphene	✓	trace	trace
8	Cu <sub>2.8</sub> Pd <sub>0.2</sub> /graphene	×	22	16
9	Cu <sub>2.8</sub> Pd <sub>0.2</sub> /graphene	×	43 <sup>d</sup>	28 <sup>e</sup>
10	none	✓	0	0
11	graphene	✓	0	0

<sup>a</sup>15 mg of catalyst was employed at 30 °C for 2 h under Xe-lamp irradiation (0.6 W/cm<sup>2</sup>) unless otherwise stated. <sup>b</sup>20 mg of catalyst was employed at 50 °C for 9 h. <sup>c</sup>Yields are based on **1a** and **1a'**, and were determined by GC–MS analysis vs. a calibrated internal standard, and are averages of two runs. <sup>d</sup>Reaction time was 10 h. <sup>e</sup>Reaction time was 48 h.

respectively. Dark reaction (without irradiation) of **1a** and **1a'** showed that the yields of **1b** with Cu<sub>3</sub>/graphene were only 12% and 7%, respectively (Table 1, entry 1). This suggests that Cu nanoparticles function as photocatalyst for the borylation, but they are insufficient. It was found that alloy nanoparticles have greater surface charge heterogeneity than monometallic nanoparticles [67–71]. The heterogeneity leads to a stronger interaction between the surface of the alloy nanoparticles and the adsorbed reactant molecules and promotes chemical transformations. Xiao and Zhu et al. achieved efficient, selective reduction of nitroaromatics using supported Ag/Cu and Au/Cu alloy nanoparticles as photocatalysts [69,70]. With this information, Pd was incorporated into plasmonic Cu nanoparticles to form a graphene-supported Cu–Pd alloy nanoparticle photocatalyst for the borylation of alkyl chlorides and bromides with B<sub>2</sub>pin<sub>2</sub>.

With both **1a** and **1a'** as substrates, the yields of **1b** over all Cu–Pd alloy catalysts are higher than those over monometallic Cu<sub>3</sub>/graphene (Table 1, entries 3–6) in air with visible light irradiation, suggesting that alloying of the two metals can greatly enhance the photocatalytic activity. Moreover, the activity depends on the ratio of Cu to Pd, with the ratio of 2.8 wt% : 0.2 wt% (Cu<sub>2.8</sub>Pd<sub>0.2</sub>/graphene, the molar ratio of Cu/Pd is 23 : 1) exhibiting optimal activity, giving **1b** in 92% yield after 2 h for **1a** and in 78% yield after 9 h for **1a'** (Table 1, entry 4). Using Pd<sub>3</sub>/graphene as the photocatalyst yielded only traces of **1b** (Table 1, entry 7), suggesting that the active phase is Cu. Dark reaction of **1a** and **1a'** yielded 22% and 16% of **1b**, respectively (Table 1, entry 8). When the dark reaction time was extended to 10 or 48 h, the yield of **1b** only increased to 43% or 28%, respectively, showing the significant contribution of visible light irradiation to the catalytic activity (Table 1, entry 9). The reaction did not occur under visible light irradiation without any catalyst, and no product was detected in control experiments using only graphene as the catalyst (Table 1, entries 10 and 11). We screened a range of solvents and bases with **1a** as substrate, and DMF and LiOtBu proved to be optimal (Table S1).

When the light intensity was reduced from 0.6 to 0.5, 0.4, 0.3, 0.2, and 0.1 W/cm<sup>2</sup> (measured through the quartz window in the reactor) while all other experimental conditions remained unchanged, the yield of 1-Bpin-3-phenylpropane (**1b**) over Cu<sub>2.8</sub>Pd<sub>0.2</sub>/graphene decreased from 92% to 82%, 74%, 62%, 50%, and 37%, respectively, indicating that the reaction was driven by the

visible light irradiation (Fig. 1A). The reduced catalytic activity is likely due to the decrease in the number of energized electrons generated at lower irradiation intensities. This approximately linear relationship indicates that the process is first order in photons, suggesting that the reaction is dominated by a single photon absorption event [72].

Fig. 1B shows the dependence of catalytic activity on the irradiation wavelength using the procedures similar to those reported in literature [58,60,61]. The yield of **1b** was 92% for the irradiation wavelength-range of 400–800 nm, 79% for 450–800 nm, 62% for 520–800 nm and 37% for 600–800 nm, respectively. As the yield of **1b** was 22% without irradiation, the light-induced conversion within each wavelength range was about 13% for 400–450 nm, 17% for 450–500 nm, 25% for 500–600 nm and 15% for 600–800 nm. Therefore, light in the wavelength-range of 400–450, 450–520, 520–600, and 600–800 nm, respectively, accounts for 18.6, 24.3, 35.7, and 21.4% of the light-induced conversion (Fig. 1B). The effect of the specific irradiation wavelength on the catalytic activity was also studied by using various LED lamps with different wavelengths. From Fig. 1C, when an LED with a wavelength of 475 ± 15 nm (light intensity = 0.3 W/cm<sup>2</sup>) was employed as the light source, the yields of **1b** were 54% in 1 h. When the wavelength was (525 ± 15), (550 ± 15), (585 ± 15), and (630 ± 15), but the light intensity was kept constant, the yield of **1b** was 63%, 76%, 57%, and 45% in 1 h, respectively. Clearly, the wavelength of light absorbed by the catalyst strongly influences the catalytic activity.

The borylation of **1a** under the irradiation of natural sunlight, with an average light intensity of 40 mW/cm<sup>2</sup> and ground temperature of 32 °C (Figure S1), was also conducted, giving a 76% yield of **1b**. The recyclability of the Cu<sub>2.8</sub>Pd<sub>0.2</sub>/graphene photocatalyst was tested by reusing it in five cycles under the same reaction conditions. The catalyst did not show any measurable loss in activity (Figure S2), indicating its excellent stability.

With the optimized reaction conditions in hand, the scope of the photocatalytic borylation reaction with different alkyl halides was examined (Table 2). Primary alkyl bromides showed high reactivity (**1b-10b**). A range of functional groups including fluorine (**5b**), ether (**6b**), and acetal (**7b**) were tolerated in the borylation reaction, with yields of the desired alkyl boronates being greater than 80%. Cyclic and acyclic secondary alkyl bromides can also be

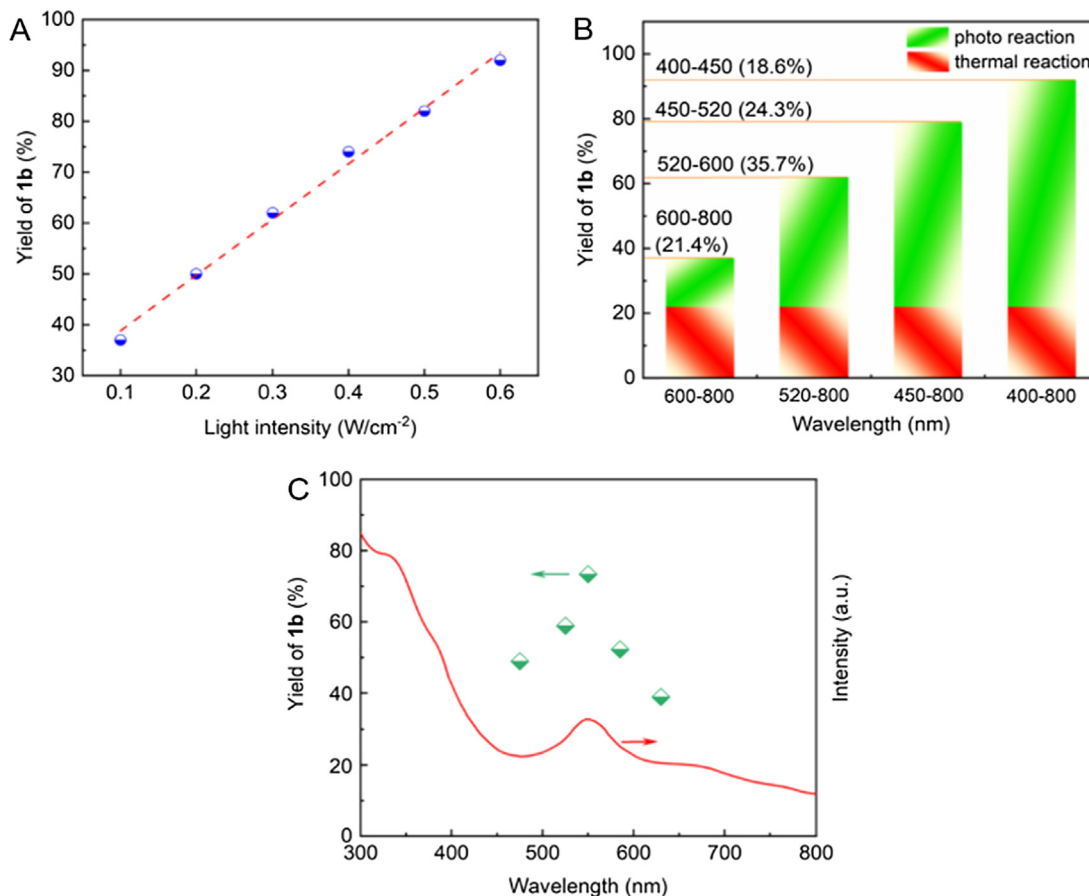


**Fig. 1.** Dependence of the catalytic activity of  $\text{Cu}_{2.8}\text{Pd}_{0.2}/\text{graphene}$  for the borylation of **1a** with  $\text{B}_2\text{pin}_2$  on the intensity (A) and wavelength (B) using a Xe lamp as the light source; (C) the effect of the specific irradiation wavelength on the catalytic activity using various LED lamps with wavelengths of  $(475 \pm 15)$ ,  $(525 \pm 15)$ ,  $(550 \pm 15)$ ,  $(585 \pm 15)$ , and  $(630 \pm 15)$  nm, respectively, and the red line in (C) is the absorption spectrum of the  $\text{Cu}_{2.8}\text{Pd}_{0.2}/\text{graphene}$  catalyst.

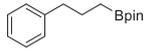
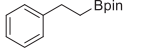
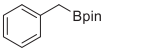
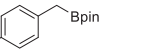
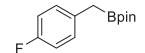
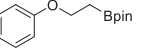
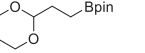
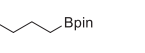
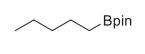
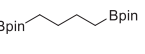
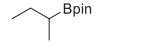
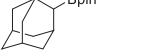
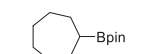
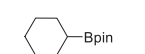
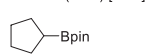
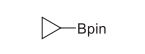
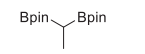
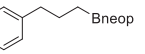
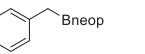
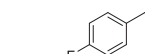
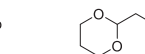
borylated in moderate yields, but the yields were greatly improved when the reactions were carried out under Ar (**11b–18b**). The  $\text{Cu}_{2.8}\text{Pd}_{0.2}/\text{graphene}$  catalyst is also effective for more readily available alkyl chlorides. Primary alkyl chlorides were converted into the corresponding alkyl boronates in good yields under air with visible light irradiation (**1b–6b**, **8b**, **9b**, **11b**, and **13b–18b**). Generally, alkyl chlorides need higher temperatures than alkyl bromides due to the respective bond strengths. For example, the C–Cl bond dissociation enthalpy in benzyl chloride is  $299.9 \pm 4.3$  kJ/mol, which is higher than that of the C–Br bond in benzyl bromide  $239.3 \pm 6.3$  kJ/mol [73]. The photocatalytic borylations of secondary alkyl chlorides conducted under Ar also gave better yields than those under air (**11b**, **13b–18b**). Employing chlorocyclobutane as an example, the borylation product **16b** was obtained in 52% and 88% under air and Ar, respectively. High yields of diborylation products were also achieved with both  $\alpha,\omega$ -dibromoalkanes (**10b**) and *gem*-dichloroalkanes (**18b**) as substrates [16,74–76]. The reaction is not limited to  $\text{B}_2\text{pin}_2$ , as bis(neopentyl glycolato)diboron ( $\text{B}_2\text{neop}_2$ ) can be used as the diboron reagent to give the corresponding alkyl boronates (**19b–23b**) with similar yields to those observed with  $\text{B}_2\text{pin}_2$ .

Preliminary mechanistic studies were performed to provide insight into the photocatalytic borylation process. We first characterized the structural features of  $\text{Cu}_{2.8}\text{Pd}_{0.2}/\text{graphene}$  catalyst. The TEM, HAADF-STEM, and HRTEM images show that the  $\text{Cu}_{2.8}\text{Pd}_{0.2}$  nanoparticles with a mean diameter of 8 nm are uniformly dispersed on graphene (Fig. 2A–D, and Figure S3). The formation of a Cu–Pd alloy was also supported by the XRD patterns (Figure S4).

Typical examples of the energy dispersive X-ray (EDX) line scan (Fig. 2C) and the high-resolution elemental mapping (Fig. 2D–H) show a homogeneous distribution of both Cu and Pd across the alloy nanoparticles. In the UV/Vis spectra (Fig. 1C, red line), the  $\text{Cu}_{2.8}\text{Pd}_{0.2}/\text{graphene}$  displays absorption in both UV and visible range. The absorption peak at 550 nm corresponds to the LSPR of Cu.

Because the electronegativity of Pd (2.20) is higher than that of Cu (1.90), a charge heterogeneity is formed at the Cu–Pd alloy nanoparticle surface [77–81]. Therefore, electrons will flow from Cu atoms to Pd atoms until the chemical potentials throughout the particle are equal. With irradiation, the conduction electrons of Cu gain incident photon energy due to the LSPR effect, yielding energetic electrons, which are also transferred to Pd [67–71,82–84]. As a result, both slightly positively charged Cu sites and electron-rich Pd sites are formed at the surface of the alloy nanoparticles, leading to interactions between these sites and electrophilic alkyl halides and nucleophilic diboron compounds being efficiently enhanced. This is revealed by the higher binding energy (BE) of Cu 2p and lower BE of Pd 3d in alloy catalyst compared with pure metal catalysts (Figure S5). Au is a well-studied plasmonic metal, and its electronegativity (2.54) is higher than those of both Pd and Cu. Therefore,  $\text{Au}_3/\text{graphene}$  and  $\text{Au}_{2.8}\text{Pd}_{0.2}/\text{graphene}$  were prepared to study the borylation of 1-bromo-3-phenylpropane (**1a**). However, no borylated product was detected with either  $\text{Au}_3/\text{graphene}$  or  $\text{Au}_{2.8}\text{Pd}_{0.2}/\text{graphene}$  as the photocatalyst. This is mainly due to two factors. 1) Au is not an effective catalyst for the borylation of alkyl halides. 2) The electronegativity difference

**Table 2**  
Scope of the photocatalytic borylation of alkyl halides.

 <b>1b</b> X = Br 92% <sup>a</sup> (85%) <sup>d</sup> [2 h] <sup>e</sup> Cl 78% <sup>b,c</sup> (70%) [9 h]	 <b>2b</b> X = Br 82% (74%) [2 h] Cl 84% <sup>b,c</sup> (75%) [8 h]	 <b>3b</b> X = Br 80% (72%) [2 h] Cl 82% <sup>b,c,f</sup> (74%) [2 h]	 <b>4b</b> X = Br 94% <sup>f</sup> (83%) [2 h] Cl 93% <sup>b,c,f</sup> (84%) [2 h]
 <b>5b</b> X = Br 97% <sup>f</sup> (88%) [2 h] Cl 95% <sup>b,c,f</sup> (85%) [2 h]	 <b>6b</b> X = Br 81% (70%) [4 h] Cl 79% <sup>b,c</sup> (71%) [20 h]	 <b>7b</b> X = Br 88% (80%) [2 h]	 <b>8b</b> X = Br 91% (84%) [2 h] Cl 85% <sup>c,f</sup> (78%) [12 h]
 <b>9b</b> X = Br 87% (80%) [2 h] Cl 81% <sup>c,f</sup> (72%) [12 h]	 <b>10b</b> X = Br 83% <sup>a</sup> (70%) [4 h]	 <b>11b</b> X = Br 71% <sup>b</sup> (64%) [3 h] Br 94% <sup>b,h</sup> (85%) [3 h] Cl 65% <sup>b,c,f</sup> (55%) [15 h] Cl 87% <sup>b,c,f,h</sup> (79%) [15 h]	 <b>12b</b> X = Br 56% <sup>b</sup> (45%) [3 h] Br 80% <sup>b,h</sup> (67%) [3 h]
 <b>13b</b> X = Br 48% <sup>b</sup> (40%) [3 h] Br 76% <sup>b,h</sup> (70%) [3 h] Cl 29% <sup>b,c,f</sup> (21%) [15 h] Cl 52% <sup>b,c,f,h</sup> (45%) [15 h]	 <b>14b</b> X = Br 57% <sup>b</sup> (50%) [3 h] Br 85% <sup>b,h</sup> (77%) [3 h] Cl 39% <sup>b,c,f</sup> (33%) [15 h] Cl 73% <sup>b,c,f,h</sup> (65%) [15 h]	 <b>15b</b> X = Br 60% <sup>b</sup> (51%) [3 h] Br 92% <sup>b,h</sup> (84%) [3 h] Cl 45% <sup>b,c,f</sup> (36%) [15 h] Cl 80% <sup>b,c,f,h</sup> (71%) [15 h]	 <b>16b</b> X = Br 63% <sup>b</sup> (54%) [3 h] Br 95% <sup>b,h</sup> (87%) [3 h] Cl 52% <sup>b,c,f</sup> (43%) [15 h] Cl 88% <sup>b,c,f,h</sup> (80%) [15 h]
 <b>17b</b> X = Br 61% <sup>b</sup> (45%) [3 h] Br 90% <sup>b,h</sup> (82%) [3 h] Cl 50% <sup>b,c,f</sup> (43%) [15 h] Cl 81% <sup>b,c,f,h</sup> (73%) [15 h]	 <b>18b</b> X = Br 56% <sup>b,g</sup> (49%) [6 h] Br 82% <sup>b,g,h</sup> (74%) [6 h] Cl 41% <sup>b,c,f,g</sup> (42%) [24 h] Cl 78% <sup>b,c,f,g,h</sup> (70%) [24 h]	 <b>19b</b> X = Br 90% <sup>b,i</sup> (82%) [4 h] Cl 84% <sup>b,i</sup> (75%) [16 h]	 <b>20b</b> X = Br 76% <sup>b,i</sup> (67%) [4 h] Cl 65% <sup>b,i</sup> (52%) [16 h]
 <b>21b</b> X = Br 80% <sup>b,i</sup> (73%) [4 h] Cl 71% <sup>b,i</sup> (62%) [16 h]	 <b>22b</b> X = Br 82% <sup>b,i</sup> (74%) [5 h]	 <b>23b</b> X = Br 53% <sup>b,i</sup> (45%) [4 h] Br 86% <sup>b,h,i</sup> (75%) [4 h] Cl 45% <sup>b,i</sup> (38%) [16 h] Cl 79% <sup>b,f,h,i</sup> (69%) [16 h]	

<sup>a</sup>Reaction conditions: 1 mmol of alkyl halide, 1.2 mmol of B<sub>2</sub>pin<sub>2</sub>, 2 mmol of LiOtBu, 15 mg of Cu<sub>2.8</sub>-Pd<sub>0.2</sub>/graphene, 10 mL of DMF, in air at 30 °C under Xe-lamp irradiation (0.6 W/cm<sup>2</sup>) unless otherwise stated. The yields are based on alkyl halides and were determined by GC–MS analysis versus a calibrated internal standard and are averages of two experiments. Isolated yields are given in parentheses and reaction times are given in square brackets. <sup>b</sup>20 mg of Cu<sub>2.8</sub>Pd<sub>0.2</sub>/graphene. <sup>c</sup>At 50 °C. <sup>d</sup>2 mmol of LiOME. <sup>e</sup>2.5 mmol of B<sub>2</sub>pin<sub>2</sub>. <sup>f</sup>Under Ar. <sup>g</sup>1.2 mmol of B<sub>2</sub>neop<sub>2</sub>.

between Pd and Au results in electron transfer from Pd to Au, forming slightly positive Pd sites, which makes Pd less effective for activating C–Br bonds.

When the photocatalytic borylation of **1a** was conducted in the presence of 1 equiv of the radical scavenger 5,5-dimethyl-1-pyrroline N-oxide (DMPO), the reaction was shut down almost completely; a similar result was also obtained using 1 equiv of 2,2,6,6-tetramethylpiperidinoxy (TEMPO), suggesting that the borylation reaction may involve a radical process. *In situ* electron paramagnetic resonance (EPR) studies of the borylation reaction of **1a** after 3 min irradiation were performed to probe the formation of radical species. Because DMPO can react with short-living radicals to generate more stable nitroxide radicals that are detectable by EPR [85], it was introduced as a spin-trap. No signal was observed in the absence of Cu<sub>2.8</sub>-Pd<sub>0.2</sub>/graphene (Fig. 3). With the catalyst, an organic radical at higher field was detected. From the simulated EPR spectrum, the parameters obtained [*g*<sub>iso</sub> = 2.0063, *a*(H) = 14.5 G, *a*(N) = 20.8 G] fit well to a nitroxide radical **1c** (Fig. 3) [86,87]. The radical **1c** shows a triplet of doublet EPR signal due to the coupling with the adjacent nitrogen and hydrogen atoms.

Thus, a photo-induced catalytic process enhances the borylation of alkyl halides with the graphene-supported Cu–Pd alloy catalyst. A

plausible explanation is as follows. Due to surface charge heterogeneity, the energetic electrons produced by LSPR light absorption of Cu transfer to Pd leading to the formation of energetic electron-rich Pd sites and slightly positive Cu sites [67,77–81]. The electron transfer from Pd to electrophilic alkyl halides generates alkyl radicals [67,88,89]. Then, the radicals react quickly with nucleophilic [B<sub>2</sub>pin<sub>2</sub>(OtBu)] formed from B<sub>2</sub>pin<sub>2</sub> with LiOtBu [11,90,91], which is adsorbed on the positively charged Cu sites, to form the final product.

#### 4. Conclusions

In conclusion, we have developed an efficient heterogeneous photocatalytic borylation of primary and secondary alkyl bromides and chlorides using graphene-supported Cu–Pd alloy nanoparticles as catalysts operating with visible light in air at 30–50 °C. The reactions proceed under mild conditions, displays a broad substrate scope and functional group tolerance. The synergistic effect of the LSPR of Cu with charge transfer from Cu to Pd due to the charge heterogeneity of the Cu–Pd alloy nanoparticles surface is critical. The cooperative effects include the transfer of energetic electrons from Pd to alkyl halides to

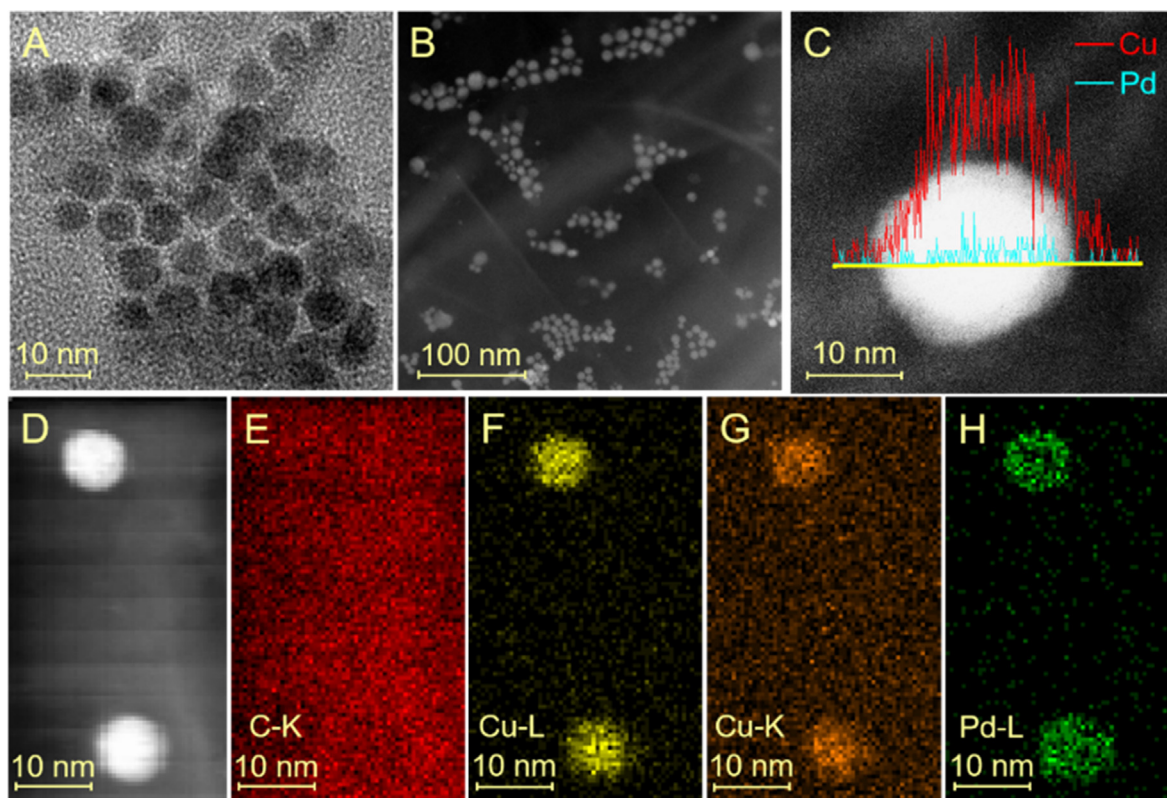


**Fig. 2.** TEM (A) and HAADF-STEM (B) images of  $\text{Cu}_{2.8}\text{Pd}_{0.2}/\text{graphene}$ ; line profile analysis of EDX spectra for a typical  $\text{Cu}_{2.8}\text{Pd}_{0.2}$  nanoparticle (C); and dark-field STEM image of two  $\text{Cu}_{2.8}\text{Pd}_{0.2}$  nanoparticles (D) and the corresponding EDX elemental maps of carbon (E), copper (F and G), and palladium (H).

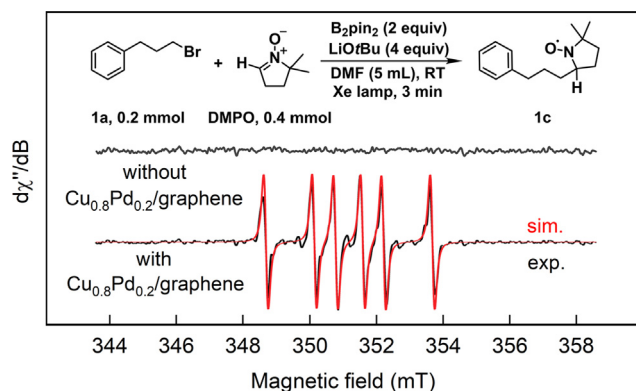


**Fig. 3.** Experimental (black) and simulated (red) EPR spectra of the borylation reaction of **1a** with and without the catalyst in the presence of DMPO after 3 min irradiation.

form alkyl radicals, and preferred adsorption of a nucleophilic adduct of a diboron compound with base on the positively charged Cu sites for reaction with the radicals generated to produce the final alkylboronic esters. The protocol developed in this study should have broad ramifications in the design of plasmonic bimetallic nanoparticle systems as photocatalysts for a wide range of organic syntheses driven by light.

#### Declaration of Competing Interest

The authors declare that they have no known competing financial interests or personal relationships that could have appeared to influence the work reported in this paper.

#### Acknowledgements

The work was financially supported by the NSFC (21673271) and the Julius-Maximilians-Universität Würzburg. Y.-M. Tian thanks the China Scholarship Council (CSC) for a PhD Scholarship, and X.-N. Guo thanks the Alexander von Humboldt Foundation for a Postdoctoral Fellowship. We thank Dr. Ivo Krummenacher for his analysis and simulation of the EPR results.

#### Appendix A. Supplementary data

Supplementary data to this article can be found online at <https://doi.org/10.1016/j.jcat.2021.01.019>.

#### References

- [1] A. Suzuki, Organoborates in new synthetic reactions, *Acc. Chem. Res.* 15 (1982) 178–184.
- [2] N. Miyaura, A. Suzuki, Palladium-Catalyzed Cross-Coupling Reactions of Organoboron Compounds, *Chem. Rev.* 95 (1995) 2457–2483.
- [3] A.D. Meijere, Metal-Catalyzed Cross-Coupling Reactions, 2nd ed., Wiley-VCH, Weinheim, 2004.
- [4] A.C. Frisch, M. Beller, Catalysts for Cross-Coupling Reactions with Non-activated Alkyl Halides, *Angew. Chem. Int. Ed.* 44 (2005) 674–688.
- [5] M.A. Beenen, C. An, J.A. Ellman, Asymmetric copper-catalyzed synthesis of alpha-amino boronate esters from N-tert-butanesulfonyl aldimines, *J. Am. Chem. Soc.* 130 (2008) 6910–6911.
- [6] I.A.I. Mkhaliid, J.H. Barnard, T.B. Marder, J.M. Murphy, J.F. Hartwig, C–H Activation for the Construction of C–B Bonds, *Chem. Rev.* 110 (2010) 890–931.
- [7] D.G. Hall, Boronic Acids: Preparation and Applications in Organic Synthesis, Medicine and Materials, 2nd ed., Wiley-VCH, Weinheim, 2011.
- [8] R. Jana, T.P. Pathak, M.S. Sigman, Advances in Transition Metal (Pd, Ni, Fe)-Catalyzed Cross-Coupling Reactions Using Alkyl-organometallics as Reaction Partners, *Chem. Rev.* 111 (2011) 1417–1492.
- [9] W.L.A. Brooks, B.S. Sumerlin, Synthesis and Applications of Boronic Acid-Containing Polymers: From Materials to Medicine, *Chem. Rev.* 116 (2016) 1375–1397.

- [10] E.C. Neeve, S.J. Geier, I.A.I. Mkhaliid, S.A. Westcott, T.B. Marder, Diboron(4) Compounds: From Structural Curiosity to Synthetic Workhorse, *Chem. Rev.* 116 (2016) 9091–9161.
- [11] C. Kleeborg, L. Dang, Z.Y. Lin, T.B. Marder, A Facile Route to Aryl Boronates: Room-Temperature, Copper-Catalyzed Borylation of Aryl Halides with Alkoxy Diboron Reagents, *Angew. Chem. Int. Ed.* 48 (2009) 5350–5354.
- [12] C.T. Yang, Z.Q. Zhang, H. Tajuddin, C.C. Wu, J. Liang, J.H. Liu, Y. Fu, M. Czyzewska, P.G. Steel, T.B. Marder, L. Liu, Alkylboronic Esters from Copper-Catalyzed Borylation of Primary and Secondary Alkyl Halides and Pseudohalides, *Angew. Chem. Int. Ed.* 51 (2012) 528–532.
- [13] H. Ito, K. Kubota, Copper(I)-Catalyzed Boryl Substitution of Unactivated Alkyl Halides, *Org. Lett.* 14 (2012) 890–893.
- [14] K. Kubota, E. Yamamoto, H. Ito, Copper(I)-Catalyzed Borylative exo-Cyclization of Alkenyl Halides Containing Unactivated Double Bond, *J. Am. Chem. Soc.* 135 (2013) 2635–2640.
- [15] H. Iwamoto, K. Kubota, E. Yamamoto, H. Ito, Copper(I)-catalyzed carbon-halogen bond-selective boryl substitution of alkyl halides bearing terminal alkene moieties, *Chem. Commun.* 51 (2015) 9655–9658.
- [16] S.K. Bose, S. Brand, H.O. Omoregie, M. Haehnel, J. Maier, G. Bringmann, T.B. Marder, Highly Efficient Synthesis of Alkylboronate Esters via Cu(II)-Catalyzed Borylation of Unactivated Alkyl Bromides and Chlorides in Air, *ACS Catal.* 6 (2016) 8332–8335.
- [17] X. Lou, Z.Q. Zhang, J.H. Liu, X.Y. Lu, Copper-catalyzed Borylation of Primary and Secondary Alkyl Halides with Bis(neopentyl glycolate) Diboron at Room Temperature, *Chem. Lett.* 45 (2016) 200–202.
- [18] J. Cui, H. Wang, J. Song, X.C. Chi, L. Meng, Q. Liu, D.P. Zhang, Y.H. Dong, H. Liu, Copper(I)-catalyzed 5-exo-trig radical cyclization/borylation of alkyl halides: access to functionalized pyrrolidine derivatives, *Org. Biomol. Chem.* 15 (2017) 8508–8512.
- [19] H. Yoshida, Y. Takemoto, S. Kamio, I. Osaka, K. Takaki, Copper-catalyzed direct borylation of alkyl, alkenyl and aryl halides with B(dan), *Org. Chem. Front.* 4 (2017) 1215–1219.
- [20] S.K. Bose, K. Fucke, L. Liu, P.G. Steel, T.B. Marder, Zinc-Catalyzed Borylation of Primary, Secondary and Tertiary Alkyl Halides with Alkoxy Diboron Reagents at Room Temperature, *Angew. Chem. Int. Ed.* 53 (2014) 1799–1803.
- [21] A.S. Dudnik, G.C. Fu, Nickel-Catalyzed Coupling Reactions of Alkyl Electrophiles, Including Unactivated Tertiary Halides, To Generate Carbon–Boron Bonds, *J. Am. Chem. Soc.* 134 (2012) 10693–10697.
- [22] J. Yi, J.H. Liu, J. Liang, J.J. Dai, C.T. Yang, Y. Fu, L. Liu, *Adv. Synth. Catal.* Alkylboronic Esters from Palladium- and Nickel-Catalyzed Borylation of Primary and Secondary Alkyl Bromides, 354 (2012), 1685–1691.
- [23] M.S. Cheung, F.K. Sheong, T.B. Marder, Z.Y. Lin, Computational Insight into Nickel-Catalyzed Carbon–Carbon versus Carbon–Boron Coupling Reactions of Primary, Secondary, and Tertiary Alkyl Bromides, *Chem. Eur. J.* 21 (2015) 7480–7488.
- [24] A. Joshi-Pangu, X. Ma, M. Diane, S. Iqbal, R.J. Kribbs, R. Huang, C.Y. Wang, M.R. Biscoe, Palladium-Catalyzed Borylation of Primary Alkyl Bromides, *J. Org. Chem.* 77 (2012) 6629–6633.
- [25] T.C. Atack, R.M. Lecker, S.P. Cook, Iron-Catalyzed Borylation of Alkyl Electrophiles, *J. Am. Chem. Soc.* 136 (2014) 9521–9523.
- [26] R.B. Bedford, P.B. Brenner, E. Carter, T. Gallagher, D.M. Murphy, D.R. Pye, Iron-Catalyzed Borylation of Alkyl, Allyl, and Aryl Halides: Isolation of an Iron(I) Boryl Complex, *Organometallics* 33 (2014) 5940–5943.
- [27] T.C. Atack, S.P. Cook, Manganese-Catalyzed Borylation of Unactivated Alkyl Chlorides, *J. Am. Chem. Soc.* 138 (2016) 6139–6142.
- [28] H.Y. Chen, J.F. Hartwig, Catalytic, Regiospecific End-Functionalization of Alkanes: Rhodium-Catalyzed Borylation under Photochemical Conditions, *Angew. Chem. Int. Ed.* 38 (1999) 3391–3393.
- [29] J.F. Hartwig, K.S. Cook, M. Hapke, C.D. Incarvito, Y. Fan, C.E. Webster, M.B. Hall, Rhodium Boryl Complexes in the Catalytic, Terminal Functionalization of Alkanes, *J. Am. Chem. Soc.* 127 (2005) 2538–2552.
- [30] A. Yoshimura, Y. Takamachi, L.B. Han, A. Ogawa, Organosulfide-Catalyzed Diboration of Terminal Alkynes under Light, *Chem. Eur. J.* 21 (2015) 13930–13933.
- [31] K. Chen, S. Zhang, P. He, P.F. Li, Efficient Metal-Free Photochemical Borylation of Aryl Halides under Batch and Continuous-Flow Conditions, *Chem. Sci.* 7 (2016) 3676–3680.
- [32] A.M. Mfuh, V.T. Nguyen, B. Chhetri, J.E. Burch, J.D. Doyle, V.N. Nesterov, H.D. Arman, O.V. Larionov, Additive- and Metal-Free, Predictably 1,2- and 1,3-Regioselective, Photoinduced Dual C–H/C–X Borylation of Haloarenes, *J. Am. Chem. Soc.* 138 (2016) 8408–8411.
- [33] A.M. Mfuh, B.D. Schneider, W. Cruces, O.V. Larionov, Metal- and additive-free photoinduced borylation of haloarenes, *Nat. Protoc.* 12 (2017) 604–610.
- [34] D.W. Hu, L.H. Wang, P.F. Li, Decarboxylative Borylation of Aliphatic Esters under Visible-Light Photoredox Conditions, *Org. Lett.* 19 (2017) 2770–2773.
- [35] S.F. Jin, O.V. Larionov, A Radical New Look for Alkene Carboboration, *Chem* 4 (2018) 1205–1207.
- [36] H. Cao, H. Jiang, H. Feng, J.M.C. Kwan, X. Liu, J. Wu, Photo-induced Decarboxylative Heck-Type Coupling of Unactivated Aliphatic Acids and Terminal Alkenes in the Absence of Sacrificial Hydrogen Acceptors, *J. Am. Chem. Soc.* 140 (2018) 16360–16367.
- [37] Y.M. Tian, X.N. Guo, M.W. Kuntze-Fechner, I. Krummenacher, H. Braunschweig, U. Radius, A. Steffen, T.B. Marder, Selective Photocatalytic C–F Borylation of Polyfluoroarenes by Rh/Ni Dual Catalysis Providing Valuable Fluorinated Arylboronate Esters, *J. Am. Chem. Soc.* 140 (2018) 17612–17623.
- [38] V.D. Nguyen, V.T. Nguyen, S. Jin, H.T. Dang, O.V. Larionov, Organoboron chemistry comes to light: Recent advances in photoinduced synthetic approaches to organoboron compounds, *Tetrahedron* 75 (2019) 584–602.
- [39] Z.F. Jiao, J.X. Zhao, X.N. Guo, X.Y. Guo, Photocatalytic C–X borylation of aryl halides by hierarchical SiC nanowire-supported Pd nanoparticles, *Chinese J. Catal.* 41 (2020) 357–363.
- [40] A. Fawcett, J. Pradeilles, Y. Wang, T. Mutsuga, E.L. Myers, V.K. Aggarwal, Photoinduced decarboxylative borylation of carboxylic acids, *Science* 357 (2017) 283–286.
- [41] J. Wu, L. He, A. Noble, V.K. Aggarwal, Photoinduced Deaminative Borylation of Alkylamines, *J. Am. Chem. Soc.* 140 (2018) 10700–10704.
- [42] Y. Cheng, C. Mgck-Lichtenfeld, A. Studer, Transition Metal-Free 1,2-Carboration of Unactivated Alkenes, *J. Am. Chem. Soc.* 140 (2018) 6221–6225.
- [43] Y. Cheng, C. Mück-Lichtenfeld, A. Studer, Metal-Free Radical Borylation of Alkyl and Aryl Iodides, *Angew. Chem. Int. Ed.* 57 (2018) 16832–16836.
- [44] F.W. Friese, A. Studer, Deoxygenative Borylation of Secondary and Tertiary Alcohols, *Angew. Chem. Int. Ed.* 58 (2019) 9561–9564.
- [45] J. Hu, G. Wang, S. Li, Z. Shi, Selective C–N Borylation of Alkyl Amines Promoted by Lewis Base, *Angew. Chem. Int. Ed.* 57 (2018) 15227–15231.
- [46] F. Sandfort, F. Strieth-Kalthoff, F. Klauck, M. James, F. Glorius, Deaminative Borylation of Aliphatic Amines Enabled by Visible Light Excitation of an Electron Donor–Acceptor Complex, *Chem. Eur. J.* 24 (2018) 17210–17214.
- [47] D. Mazzarella, G. Magagnano, B. Schweitzer-Chaput, P. Melchiorre, Photochemical Organocatalytic Borylation of Alkyl Chlorides, Bromides, and Sulfonates, *ACS Catal.* 9 (2019), 5876–5880.14.
- [48] Q. Liu, J. Hong, B. Sun, G. Bai, F. Li, G. Liu, Y. Yang, F. Mo, Transition-Metal-Free Borylation of Alkyl Iodides via a Radical Mechanism, *Org. Lett.* 21 (2019) 6597–6602.
- [49] L. Zhang, Z.Q. Wu, L. Jiao, Photoinduced Radical Borylation of Alkyl Bromides Catalyzed by 4-Phenylpyridine, *Angew. Chem. Int. Ed.* 59 (2020) 2095–2099.
- [50] A. Bej, D. Srimani, A. Sarkar, Palladium nanoparticle catalysis: borylation of aryl and benzyl halides and one-pot biaryl synthesis via sequential borylation–Suzuki–Miyaura coupling, *Green Chem.* 14 (2012) 661–667.
- [51] J.H. Kim, Y.K. Chung, Copper nanoparticle-catalyzed borylation of alkyl bromides with an organodiboron compound, *RSC Adv.* 4 (2014) 39755–39758.
- [52] X.F. Zhou, Y.D. Wu, J.J. Dai, Y.J. Li, Y. Huang, H.J. Xu, Borylation of primary and secondary alkyl bromides catalyzed by Cu<sub>2</sub>O nanoparticles, *RSC Adv.* 5 (2015) 46672–46676.
- [53] M.L. Shegavi, A. Agarwal, S.K. Bose, Efficient synthesis of alkylboronic esters via magnetically recoverable copper nanoparticle-catalyzed borylation of alkyl chlorides and bromides, *Green Chem.* 22 (2020) 2799–2803.
- [54] P.K. Verma, M.L. Shegavi, S.K. Bose, K. Geetharani, A nano-catalytic approach for C–B bond formation reactions, *Org. Biomol. Chem.* 16 (2018) 857–873.
- [55] H.Y. Zhu, X.B. Ke, X.Z. Yang, S. Sarina, H.W. Liu, Reduction of nitroaromatic compounds on supported gold nanoparticles by visible and ultraviolet light, *Angew. Chem. Int. Ed.* 49 (2010) 9657–9661.
- [56] S. Lincic, P. Christopher, D.B. Ingram, Plasmonic-metal nanostructures for efficient conversion of solar to chemical energy, *Nat. Mater.* 10 (2011) 911–921.
- [57] A. Marimuthu, J.W. Zhang, S. Lincic, Tuning Selectivity in Propylene Epoxidation by Plasmon Mediated Photo-Switching of Cu Oxidation State, *Science* 339 (2013) 1590–1593.
- [58] X.N. Guo, C.H. Hao, G.Q. Jin, H.Y. Zhu, X.Y. Guo, Copper Nanoparticles on Graphene Support: An Efficient Photocatalyst for Coupling of Nitroaromatics in Visible Light, *Angew. Chem. Int. Ed.* 53 (2014) 1973–1977.
- [59] X.J. Lang, X.D. Chen, J.C. Zhao, Heterogeneous visible light photocatalysis for selective organic transformations, *Chem. Soc. Rev.* 43 (2014) 473–486.
- [60] Z.Y. Zhai, X.N. Guo, G.Q. Jin, X.Y. Guo, Visible light-induced selective photocatalytic aerobic oxidation of amines into imines on Cu/graphene, *Catal. Sci. Technol.* 5 (2015) 4202–4207.
- [61] Y.L. Cui, X.N. Guo, Y.Y. Wang, X.Y. Guo, Visible-light-driven Photocatalytic N-arylation of Imidazole Derivatives and Arylboronic Acids on Cu/graphene catalyst, *Sci. Rep.* 5 (2015) 12005.
- [62] Y.M. Huang, Z. Liu, G.P. Gao, G. Xiao, A.J. Du, S. Bottle, S. Sarina, H.Y. Zhu, Stable Copper Nanoparticle Photocatalysts for Selective Epoxidation of Alkenes with Visible Light, *ACS Catal.* 7 (2017) 4975–4985.
- [63] U. Aslam, V.G. Rao, S. Chavez, S. Lincic, Catalytic conversion of solar to chemical energy on plasmonic metal nanostructures, *Nat. Catal.* 1 (2018) 656–665.
- [64] V. Kurnaravel, S. Mathew, J. Bartlett, S.C. Pillai, Photocatalytic hydrogen production using metal doped TiO<sub>2</sub>: A review of recent advances, *Appl. Catal. B* 244 (2019) 1021–1064.
- [65] Z.J. Wang, H. Song, H. Pang, Y.X. Ning, T.D. Dao, Z. Wang, H.H. Chen, Y.X. Weng, Q. Fu, T. Nagao, Y.M. Fang, J.H. Ye, Photo-assisted methanol synthesis via CO<sub>2</sub> reduction under ambient pressure over plasmonic Cu/ZnO catalysts, *Appl. Catal. B* 250 (2019) 10–16.
- [66] P.F. Han, T. Tana, Q. Xiao, S. Sarina, E.R. Waclawik, D.E. Gómez, H.Y. Zhu, Promoting Ni(II) Catalysis with Plasmonic Antennas, *Chem* 5 (2019) 2879–2899.
- [67] S. Sarina, H.Y. Zhu, E. Jaatinen, Q. Xiao, H.W. Liu, J.F. Jia, C. Chen, J. Zhao, Enhancing Catalytic Performance of Palladium in Gold and Palladium Alloy Nanoparticles for Organic Synthesis Reactions through Visible Light Irradiation at Ambient Temperatures, *J. Am. Chem. Soc.* 135 (2013) 5793–5801.
- [68] Q. Kang, T. Wang, P. Li, L.Q. Liu, K. Chang, M. Li, J.H. Ye, Photocatalytic Reduction of Carbon Dioxide by Hydrous Hydrazine over Au–Cu Alloy

- Nanoparticles Supported on SrTiO<sub>3</sub>/TiO<sub>2</sub> Coaxial Nanotube Arrays, *Angew. Chem. Int. Ed.* 54 (2015) 841–845.
- [69] Z. Liu, Y.M. Huang, Q. Xiao, H.Y. Zhu, Selective reduction of nitroaromatics to azoxy compounds on supported Ag-Cu alloy nanoparticles through visible light irradiation, *Green Chem.* 18 (2016) 817–825.
- [70] Q. Xiao, S. Sarina, E.R. Waclawik, J.F. Jia, J. Chang, J.D. Riches, H.S. Wu, Z.F. Zheng, H.Y. Zhu, Alloying Gold with Copper Makes for a Highly Selective Visible-Light Photocatalyst for the Reduction of Nitroaromatics to Anilines, *ACS Catal.* 6 (2016) 1744–1753.
- [71] U. Aslam, S. Chavez, S. Linic, Controlling energy flow in multimetallic nanostructures for plasmonic catalysis, *Nat. Nanotechnol.* 12 (2017) 1000–1005.
- [72] M.J. Kale, T. Avanesian, P. Christopher, Direct Photocatalysis by Plasmonic Nanostructures, *ACS Catal.* 4 (2014) 116–128.
- [73] S.P. Verevkin, E.L. Krasnykh, J.S. Wright, Thermodynamic properties of benzyl halides: enthalpies of formation, strain enthalpies, and carbon–halogen bond dissociation enthalpies, *Phys. Chem. Chem. Phys.* 5 (2003) 2605–2611.
- [74] Z.Q. Zhang, C.T. Yang, L.J. Liang, B. Xiao, X. Lu, J.H. Liu, Y.Y. Sun, T.B. Marder, Y. Fu, Copper-Catalyzed/Promoted Cross-coupling of gem-Diborylalkanes with Nonactivated Primary Alkyl Halides: An Alternative Route to Alkylboronic Esters, *Org. Lett.* 16 (2014) 6342–6345.
- [75] R. Nallagonda, K. Padala, A. Masarwa, gem-Diborylalkanes: recent advances in their preparation, transformation and application, *Org. Biomol. Chem.* 16 (2018) 1050–1064.
- [76] L. Wang, T. Zhang, W. Sun, Z.Y. He, C.G. Xia, Y. Lan, C. Liu, C–O Functionalization of  $\alpha$ -Oxyboronates: A Deoxygenative gem-Diborylation and gem-Silylborylation of Aldehydes and Ketones, *J. Am. Chem. Soc.* 139 (2017) 5257–5264.
- [77] R. Ferrando, J. Jellinek, R.L. Johnston, Nanoalloys: From Theory to Applications of Alloy Clusters and Nanoparticles, *Chem. Rev.* 108 (2008) 845–910.
- [78] X.Y. Wang, R.Y. Wang, J. Wang, C.Y. Fan, Z.F. Zheng, The synergistic role of the support surface and Au-Cu alloys in a plasmonic Au-Cu@LDH photocatalyst for the oxidative esterification of benzyl alcohol with methanol, *Phys. Chem. Chem. Phys.* 22 (2020) 1655–1664.
- [79] D. Chen, P.C. Sun, H. Liu, J. Yang, Bimetallic Cu-Pd alloy multipods and their highly electrocatalytic performance for formic acid oxidation and oxygen reduction, *J. Mater. Chem. A* 5 (2017) 4421–4429.
- [80] Y.L. Zheng, S.L. Zhao, S.L. Liu, H.H. Yin, Y.Y. Chen, J.C. Bao, M. Han, Z.H. Dai, Component-Controlled Synthesis and Assembly of Cu-Pd Nanocrystals on Graphene for Oxygen Reduction Reaction, *ACS Appl. Mater. Interfaces* 7 (2015) 5347–5357.
- [81] F. Shahvaranfard, P. Ghigna, A. Minguzzi, E. Wierzbicka, P. Schmuki, M. Altomare, Dewetting of PtCu Nanoalloys on TiO<sub>2</sub> Nanocavities Provides a Synergistic Photocatalytic Enhancement for Efficient H<sub>2</sub> Evolution, *ACS Appl. Mater. Interfaces* 12 (2020) 38211–38221.
- [82] D. Wang, H.L. Xin, R. Hovden, H. Wang, Y. Yu, D.A. Muller, F.J. DiSalvo, H.D. Abruña, Structurally ordered intermetallic platinum-cobalt core-shell nanoparticles with enhanced activity and stability as oxygen reduction electrocatalysts, *Nat. Mater.* 12 (2013) 81–87.
- [83] M.K. Kumar, J.Y. Do, A.K. Reddy, M. Kang, Natural solar light-driven preparation of plasmonic resonance-based alloy and core-shell catalyst for sustainable enhanced hydrogen production: Green approach and characterization, *Appl. Catal. B* 231 (2018) 137–150.
- [84] E. Peiris, S. Sarina, E.R. Waclawik, G.A. Ayoko, P.F. Han, J.F. Jia, H.Y. Zhu, Plasmonic Switching of the Reaction Pathway: Visible-Light Irradiation Varies the Reactant Concentration at the Solid-Solution Interface of a Gold-Cobalt Catalyst, *Angew. Chem. Int. Ed.* 58 (2019) 12032–12036.
- [85] G.R. Buettner, Spin trapping: ESR parameters of spin adducts, *Free Radical Biol. Med.* 3 (1987) 259–303.
- [86] E.G. Janzen, J.I.P. Liu, Radical addition reactions of 5,5-Dimethyl-1-pyrroline-1-oxide. ESR spin trapping with a cyclic nitron, *J. Magn. Reson.* 9 (1973) 510–512.
- [87] E.G. Janzen, C.A. Evans, J.I.P. Liu, Nitrogen-14 nuclear magnetic resonance of the amino terminal group of leu-enkephalin in aqueous solution, *J. Magn. Reson.* 9 (1973) 513–516.
- [88] Z.F. Jiao, Z.Y. Zhai, X.N. Guo, X.Y. Guo, Visible-Light-Driven Photocatalytic Suzuki-Miyaura Coupling Reaction on Mott-Schottky-type Pd/SiC Catalyst, *J. Phys. Chem. C* 119 (2015) 3238–3243.
- [89] Z.F. Jiao, Y.M. Tian, B. Zhang, C.H. Hao, Y. Qiao, Y.X. Wang, Y. Qin, U. Radius, H. Braunschweig, T.B. Marder, X.N. Guo, X.Y. Guo, High photocatalytic activity of a NiO nanodot-decorated Pd/SiC catalyst for the Suzuki-Miyaura cross-coupling of aryl bromides and chlorides in air under visible light, *J. Catal.* 389 (2020) 517–524.
- [90] S. Pietsch, E.C. Neeve, D.C. Apperley, R. Bertermann, F. Mo, D. Qiu, M.S. Cheung, L. Dang, J. Wang, U. Radius, Z.Y. Lin, C. Kleeborg, T.B. Marder, Synthesis, Structure, and Reactivity of Anionic sp<sup>2</sup>-sp<sup>3</sup> Diboron Compounds: Readily Accessible Boryl Nucleophiles, *Chem. Eur. J.* 21 (2015) 7082–7098.
- [91] R.D. Dewhurst, E.C. Neeve, H. Braunschweig, T.B. Marder, sp<sup>2</sup>-sp<sup>3</sup> diboranes: astounding structural variability and mild sources of nucleophilic boron for organic synthesis, *Chem. Commun.* 51 (2015) 9594–9607.